



## Structural and optical nanoscale analysis of GaN core–shell microrod arrays fabricated by combined top-down and bottom-up process on Si(111)

Marcus Müller<sup>1,2\*</sup>, Gordon Schmidt<sup>1</sup>, Sebastian Metzner<sup>1</sup>, Peter Veit<sup>1</sup>, Frank Bertram<sup>1</sup>, Sergiy Krylyuk<sup>2,4</sup>, Ratan Debnath<sup>2,5</sup>, Jong-Yoon Ha<sup>2,4</sup>, Baomei Wen<sup>2,5</sup>, Paul Blanchard<sup>3</sup>, Abhishek Motayed<sup>2,4,5</sup>, Matthew R. King<sup>6</sup>, Albert V. Davydov<sup>2</sup>, and Jürgen Christen<sup>1</sup>

<sup>1</sup>Institute of Experimental Physics, Otto-von-Guericke-University Magdeburg, 39106 Magdeburg, Germany

<sup>2</sup>Materials Science and Engineering Division, National Institute of Standards and Technology, Gaithersburg, MD 20899, U.S.A.

<sup>3</sup>Quantum Electronics and Photonics Division, National Institute of Standards and Technology, Boulder, CO 80305, U.S.A.

<sup>4</sup>Institute for Research in Electronics and Applied Physics, University of Maryland, College Park, MD 20742, U.S.A.

<sup>5</sup>N5 Sensors Inc., Rockville, MD 20852, U.S.A.

<sup>6</sup>Northrop Grumman ES, Linthicum, MD 21090, U.S.A.

\*E-mail: marcus.mueller@ovgu.de

Received November 5, 2015; accepted December 28, 2015; published online March 30, 2016

Large arrays of GaN core–shell microrods were fabricated on Si(111) substrates applying a combined bottom-up and top-down approach which includes inductively coupled plasma (ICP) etching of patterned GaN films grown by metal–organic vapor phase epitaxy (MOVPE) and selective overgrowth of obtained GaN/Si pillars using hydride vapor phase epitaxy (HVPE). The structural and optical properties of individual core–shell microrods have been studied with a nanometer scale spatial resolution using low-temperature cathodoluminescence spectroscopy (CL) directly performed in a scanning electron microscope (SEM) and in a scanning transmission electron microscope (STEM). SEM, TEM, and CL measurements reveal the formation of distinct growth domains during the HVPE overgrowth. A high free-carrier concentration observed in the non-polar {1100} HVPE shells is assigned to in-diffusion of silicon atoms from the substrate. In contrast, the HVPE shells directly grown on top of the c-plane of the GaN pillars reveal a lower free-carrier concentration. © 2016 The Japan Society of Applied Physics

### 1. Introduction

Three-dimensional GaN based core–shell microrods provide a promising material system to improve the performance of optoelectronic devices.<sup>1,2</sup> Potential benefits of microrod heterostructures as light emitters and photodetectors rely on the core–shell geometry which results in an increased optically active area in comparison to conventional planar structures.<sup>3,4</sup> Besides, microrods offer an enhanced light extraction efficiency and a reduction of the spontaneous polarization fields due to the formation of non-polar side-walls.<sup>5</sup> Various approaches for the fabrication of nano- and microrod GaN heterostructures have been presented by different growth techniques such as molecular beam epitaxy (MBE),<sup>6,7</sup> metal–organic vapor phase epitaxy (MOVPE)<sup>8,9</sup> and hydride vapor phase epitaxy (HVPE).<sup>10,11</sup> In particular, the HVPE offers the advantage of high growth rates, which can be applied to achieve a high aspect ratio of the microrod heterostructures. However, a precise control of growth of the nanostructures is necessary. Combining HVPE and selective area epitaxy (SAE) by using a two-step fabrication process with a bottom-up and top-down approach allows direct control of the growth, e.g., size, position, and alloy composition of the core–shell layer structure. Furthermore, uniformity of large areas and a scalable fabrication process can be achieved by this method. Another key development for high efficient optoelectronic devices is the integration with low cost silicon substrates. Nevertheless, the realization of three-dimensional nanostructure devices requires a careful investigation of the morphology, the crystal quality as well as the optical and electrical properties of the core–shell structures.

In this paper, we present a detailed nano-scale analysis of individual GaN core–shell microrods fabricated by a combined top-down down and bottom-up approach on Si(111) by using highly spatially resolved cathodolumines-

cence (CL) spectroscopy directly performed in a scanning electron microscope (SEM) and in a scanning transmission electron microscope (STEM).

### 2. Experimental methods

The two-step fabrication process of GaN core–shell microrods consists of inductively coupled plasma (ICP) etching of lithographically patterned GaN-on-Si templates followed by selective area epitaxial growth of GaN shells using HVPE. In the first step, a 0.8 μm thick Si-doped GaN(0001) layer was grown on 4-in. Si(111) substrate with a grading AlGaIn buffer layer by MOVPE. Then the wafers were patterned using deep UV lithography and metal mask lift-off, followed by ICP and hot-phosphoric-acid (PA) etching to fabricate regular 5 × 5 mm<sup>2</sup> arrays of 2 μm diameter GaN-on-Si micropillars with a mean density of 8.8 × 10<sup>5</sup> cm<sup>-2</sup>. Subsequently, the micropillars were overgrown with the undoped GaN epilayers by selective area HVPE at 950 °C. Further information on growth conditions and processing can be found in Refs. 11–13. The schematic drawing of the core–shell microrod heterostructure is shown in Fig. 1(a).

The morphology of the GaN microrods was examined using a secondary electron microscope JEOL JSM 7100 FT with an integrated Nordly electron backscatter diffraction (EBSD) detector from Oxford Instruments.<sup>14</sup> Low-temperature CL imaging was carried out at  $T = 6$  K in a modified JEOL 6400 SEM previously used to study optical properties of GaN microstructures with a nanoscale spatial resolution.<sup>15,16</sup> The SEM-CL measurements were operated at 5 keV and an electron-beam current of 900 pA. The crystalline structure of the microrods was investigated by STEM-CL in a FEI STEM Tecnai F20 equipped with a liquid helium stage ( $T < 15$  K) and a CL detection unit (Gatan MONO CL4). The STEM-CL measurements were performed at 80 kV acceleration voltage to minimize sample damage and prevent luminescence degradation. For STEM-CL experiments, a

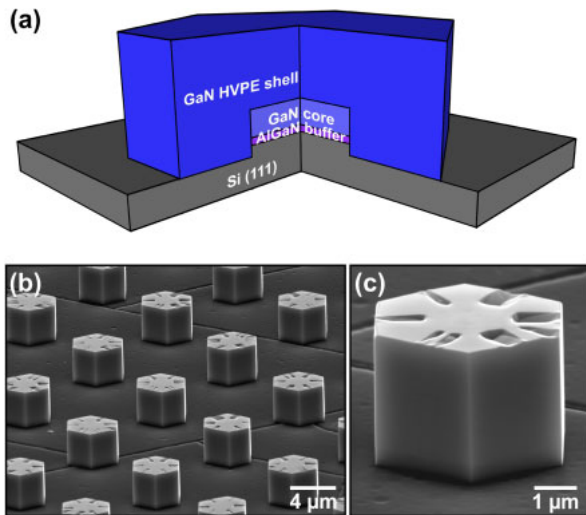


**Fig. 1.** (Color online) (a) Schematic drawing of the microrod core-shell heterostructures. The SEM image (b) of the GaN microrod array on Si(111) shows a homogeneous overgrowth of the initial GaN pillars. The SEM image of single microrod in (c) reveals the formation of vertical non-polar side walls and *c*-plane top facet truncated by high-index vicinal facets.

single microrod from the ensemble has been prepared in cross-section using a Zeiss Auriga focused ion beam SEM. An optimized focused ion beam (FIB) preparation process was applied to thin the sample to electron transparency. The FIB acceleration voltage was reduced from 30 to 5 kV in the last step to prevent surface degradation. More detailed information about the experimental method and the preparation can be found elsewhere.<sup>17,18)</sup>

### 3. Results and discussion

Figure 1(b) shows a representative SEM image of an array of the GaN core-shell microrods. The sample was oriented in 45° to study the morphology of the three-dimensional heterostructures. SEM measurements of the epitaxially overgrown samples reveal a homogeneous HVPE growth of the GaN shell layer over the entire 25 mm<sup>2</sup> chip. The HVPE growth occurs selectively on the etched pillars. No residual GaN growth is found between the microrods on the Si substrate. The HVPE overgrowth of the GaN pillars results in hexagonally shaped microrods. The orientation control of the sidewall facets by employing a phosphoric acid etch of the ICP-etched pillars and by tuning the HVPE growth conditions has been recently reported by Krylyuk et al.<sup>13)</sup> Due to the large lattice and thermal mismatch of GaN and Si(111), cracks in the GaN film are generated down to the Si substrate during the initial MOVPE growth process, as previously observed by Dadgar et al.<sup>19)</sup> The epitaxial HVPE overgrowth of the ICP etched GaN pillars however is not affected by the cracking. The SEM image of a single microrod is depicted in Fig. 1(c). The average diameter and height of the complete microrod structure was measured to be 3.3 and 4.5 μm, respectively. One can clearly see that overgrown GaN shell layer contacts the Si substrate. Electron-backscattered diffraction (not shown) confirmed that the vertical sidewalls are non-polar {1100} planes. Typically, the top *c*-plane surface shows grooves with high index facets.

Highly spatially resolved CL investigations under 45° tilt geometry in bird's eye view have been carried out to correlate

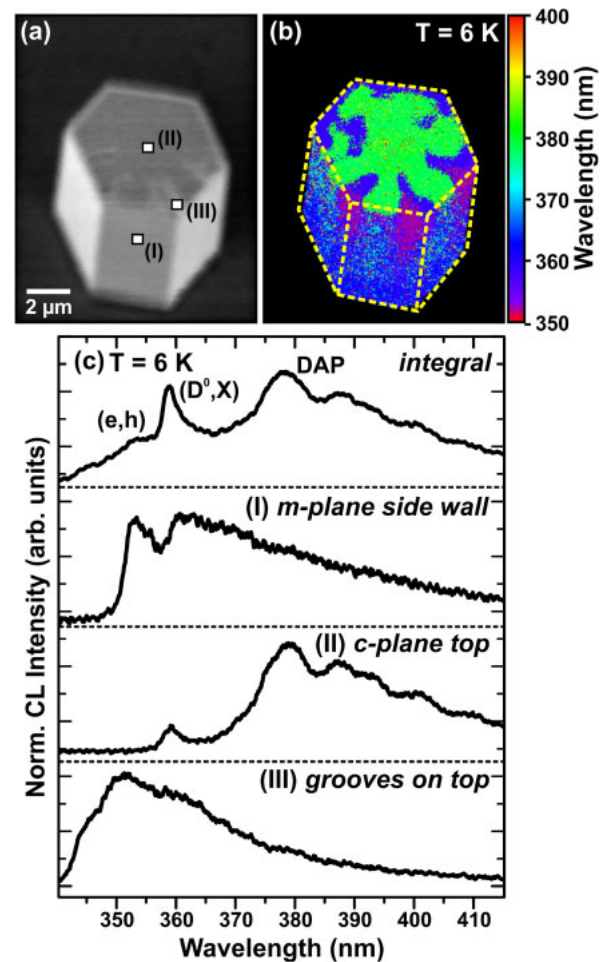


**Fig. 2.** (Color online) SEM image (a) and CLWI (b) of a single microrod in bird's eye view. The CLWI shows clearly the different recombination channels from the different microrod regions. The spatially integrated spectrum and the local spectra in (c) from the different growth regions exhibit the donor-bound exciton emission, the DAP transition and the broad blue shifted free electron-hole recombination.

the optical and structural properties of GaN microrods. The SEM image of a single microrod is depicted in Fig. 2(a) showing the *m*-plane side walls and the top polar facet. In Fig. 2(b), the corresponding color-coded CL wavelength image (CLWI) is mapping the local peak positions and directly visualizes three different growth domains: the non-polar side-walls, the *c*-plane top facet, and the high index facets on the top *c*-plane. The microrod shape from the SEM image is marked as a yellow dashed line in the CLWI. The spatially integrated CL spectrum from the microrod [Fig. 2(c)] exhibits donor-bound exciton luminescence at 358 nm, which is slightly red shifted with respect to the value of the relaxed undoped GaN. The full width at half maximum (FWHM) of the exciton emission line is 40 meV. Such a large value of the FWHM could be partially due to the spatial integration of CL over the entire microrod. A broad blue shifted emission band at 353 nm appears on the high-energy shoulder of the excitonic luminescence. This blue shifted emission has been observed by other groups for HVPE GaN structures and is attributed to free electron-hole (*e,h*) recombination caused by a locally high free-carrier concentration.<sup>20–22)</sup> Feneberg et al. have shown that free-carrier recombination processes are efficient in heavily doped GaN layers.<sup>23)</sup> Also, a CL contribution from the donor-acceptor

pair (DAP) recombination at 378 nm with longitudinal-optical (LO) phonon replica is observed.

In detail, the optical properties of the different regions of a single microrod have been studied by local CL spectra [Fig. 2(c) positions I–III]. The *m*-plane side facets exhibit extremely red shifted excitonic emission at about 361 nm [Fig. 2(c), position I]. The red shift of excitonic emission is caused by biaxial tensile strain of the microrod shell<sup>20)</sup> and/or bandgap renormalization (BGR) due to unintentionally doping during the HVPE overgrowth.<sup>21)</sup> The BGR leads to a decrease of the fundamental band gap energy with increasing carrier density due to electron–electron and electron–ion interaction.<sup>22)</sup> In addition to the red shifted excitonic emission, the non-polar facets reveal an intense CL line at 352 nm assigned to (e,h) recombination. This may indicate a high density of impurities incorporated locally in the GaN shell during the epitaxial overgrowth. The generated free carriers in the shell can diffuse to these regions with high impurity concentration and recombine there. Due to the formation of local regions with high free-carrier concentration in the shell, the excitonic emission as well as the (e,h) transition appear in the local spectrum. In-diffusion of silicon from the substrate and unintentionally doping with oxygen during the HVPE process of the GaN shell are typical sources of the impurities which lead to high free-carrier concentration.<sup>24)</sup> The free-carrier concentration in the non-polar shell is estimated from the spectrum to be locally higher than  $10^{18} \text{ cm}^{-3}$  according to Refs. 21 and 22.

The top *c*-plane facet (position II) shows an intense DAP transition with zero phonon line centered at 378 nm and LO-phonon replicas on the longer wavelength side. In addition, the excitonic emission appears at 358 nm in the local spectrum from defect free part of the top facet, i.e., away from the grooves. This implies a lower incorporation of impurities in the growing *c*-plane of the microrod compared to the non-polar shell. According to the previous study, the phosphoric acid etch of the GaN pillars causes the HVPE shell growth to start simultaneously on the top of the pillars as well as at the Si–GaN interface.<sup>13)</sup> This results in different growth fronts moving in the [0001],  $\langle 1\bar{1}01 \rangle$ , and  $\langle 1\bar{1}00 \rangle$  directions. Hence, more Si atoms from the substrate can diffuse during the HVPE growth process to the non-polar sidewalls in comparison to the top facet. At the grooves on the top facet of the microrod, we observe exclusively a broad luminescence band from the free-electron recombination process (position III) which may imply very efficient incorporation of impurities.

To correlate the nanoscopic crystal structure of the MOVPE core and the HVPE shell with local luminescence properties, low-temperature CL microscopy was carried out directly in a STEM on cross-section of a single microrod sample prepared by FIB [Figs. 3(a) and 3(b)]. The bright-field STEM image shown in Fig. 3(a) reveals a high dislocation density in the MOVPE GaN core caused by a large lattice mismatch between GaN and the Si substrate (appears as bright contrast in the bottom of the image). The GaN shell grown by HVPE is wrapped around the initial ICP etched GaN pillar and extends below the original interface between the GaN pillar and the Si substrate. Most of the dislocations generated at the AlGaIn/Si interface propagate vertically along the [0001] direction into the HVPE shell

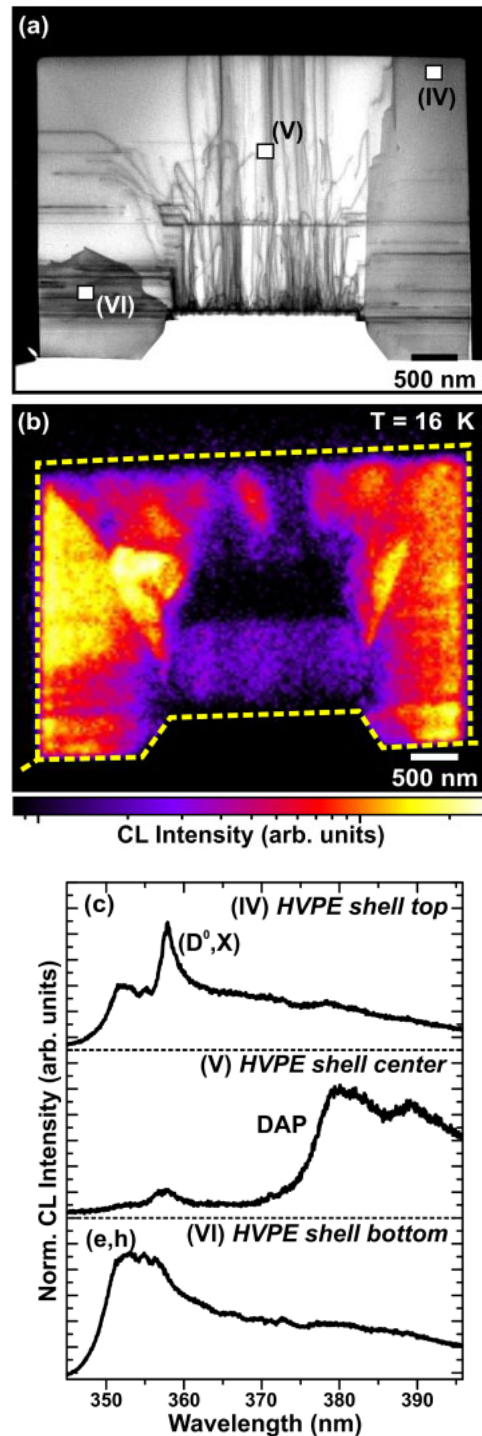


**Fig. 3.** (Color online) The cross-sectional bright-field STEM image (a) exhibits the core–shell structure of the microrod. The corresponding panchromatic CL intensity image (b) taken at 16 K reveals a weak luminescence from the MOVPE GaN pillar and the HVPE shell grown directly on top of the pillar due to a high density of TDs. Local spectra (c) from the different growth domains indicate increased free-carrier concentration in the non-polar HVPE shell.

grown on the top facet of the etched pillar. Some of the dislocations bend by 90° from their initial propagation direction and propagate into the laterally growing shell. The bending of dislocations is frequently observed in GaN epitaxial lateral overgrowth.<sup>25,26)</sup> The non-polar sidewall is formed by lateral growth, whereas GaN on top of the MOVPE template is grown coherently in the polar direction. The bright field STEM image shows clearly a strong

reduction of the dislocation density in the laterally grown portion of the GaN shell which indicates an improved crystal quality. Basal plane stacking faults (BSF) are generated near the bottom of the GaN shell in the close vicinity to the Si substrate. The BSFs propagate towards  $\{1\bar{1}00\}$  sidewalls where they are terminated.

The panchromatic CL intensity image shown in Fig. 3(b) reveals a weak luminescence from the MOVPE core which correlates with a high dislocation density observed in STEM. The GaN layer grown on top of the AlGaIn shows a lower defect density and consequently an increased luminescence. Nevertheless, non-radiative recombination processes at threading dislocations in the GaN MOVPE core reduce the panchromatic intensity. The GaN grown by HVPE coherently on top of the MOVPE core exhibits a weak luminescence as well because most of the TDs run from the core into the shell, as seen in the STEM image, resulting in quenching of the luminescence in the shell. However, in the upper portion of the HVPE shell, a recovery of the CL intensity is observed due to a reduction of defect density. In contrast, the HVPE shell grown laterally in the non-polar directions shows the highest CL intensity which corresponds to the lowest TD density. The intensity distribution in bottom part of the HVPE shell exhibits a stripe-like contrast elongated along the  $[1\bar{1}00]$  direction. Here, TDs bent from the center of the structure propagate toward the  $m$ -plane surface and thus lead to a reduction of the luminescence in consequence of non-radiative recombination processes of the generated carriers.

The local CL spectra in Fig. 3(c) clearly visualize a variation of the luminescence properties in different growth domains. At the very top of the laterally grown portion of the shell (position IV), an intense donor-bound exciton luminescence at 358 nm is detected indicating a high crystal quality and low impurity incorporation. In comparison, the most intense CL line in the center of the HVPE shell is caused by DAP recombination (position V). Finally, at the base of the shell (position VI) the free-carrier concentration becomes so significant that the spectrum is dominated by the free-electron recombination rather than by excitonic emission. The cross-section investigations clearly correspond with the CL measurements on the as-grown microrods (Fig. 2). We assume that the dominance of the different recombination channels in different growth domains is caused by a varying free-carrier concentration within the shell.

A direct visualization of the different free-carrier concentration within the GaN shell grown in the non-polar direction and in the layer grown on top of the MOVPE template is evident from the CL linescans shown in Fig. 4. The vertical CL linescan presented in Fig. 4(a) was acquired in the center of the microrod. The CL linescan starts at the Si(111)/AlGaIn interface and goes through the MOVPE core to the HVPE shell and finally ends at the surface of the microrod. Within the GaN core, the CL spectrum is dominated by the excitonic emission at 357 nm, indicating strain-free MOVPE template. Usually, GaN layers grown on Si are under biaxial tensile-strain, which leads to a red shift of the exciton luminescence.<sup>27)</sup> However, the strain partially relaxes in the ICP-etched GaN pillar, as previously shown by Raman and photoluminescence studies.<sup>11)</sup> A contribution of the yellow luminescence (YL) within the MOVPE core can also be seen in the linescan, as often observed for GaN layers.<sup>28,29)</sup> An

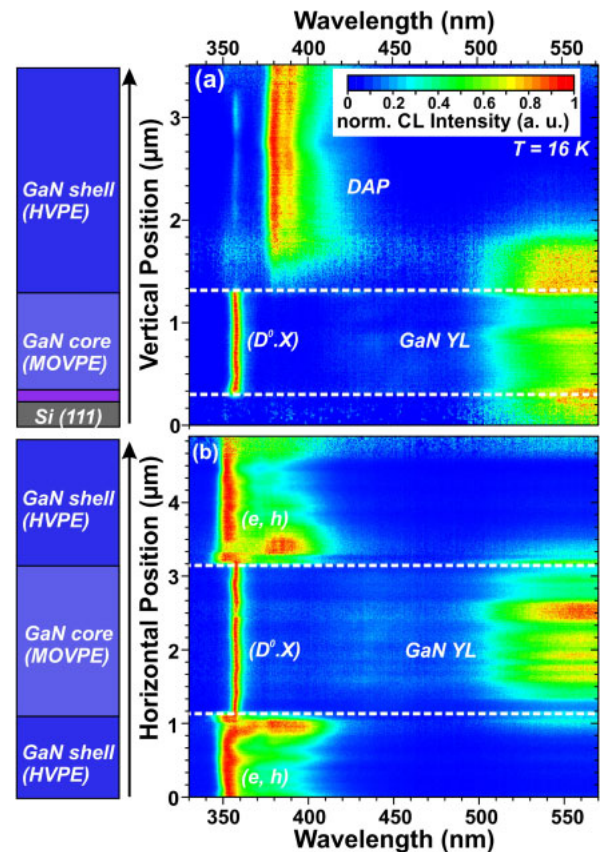


**Fig. 4.** (Color online) Vertical (a) and horizontal (b) CL linescans across the core-shell structure with the corresponding schematic drawing indicating the scan direction. The vertical CL linescan (a) stems from the center of the microrod. The horizontal CL linescan (b) was performed across the GaN HVPE shell and the MOVPE template in the middle part of the microrod. The CL spectra at the bottom and top parts of the non-polar sidewalls are dominated by the (e,h) and DAP transitions, respectively.

abrupt change of the optical properties appears at the interface of the MOVPE core/HVPE shell. The HVPE shell exhibits a strong CL at 378 nm from DAP transitions whereas CL intensity of the excitonic transitions is reduced in comparison to the underlying core. The YL disappears in the upper part of the HVPE shell. The horizontal linescan in Fig. 4(b) was obtained from the middle part of the microrod across the GaN HVPE shell and the MOVPE template. Unlike the vertical linescan, the horizontal linescan in the vicinity of the HVPE shell [Fig. 4(b)] shows a broad blue shifted emission band due to the (e,h) recombination indicating a locally high incorporation of impurities during the overgrowth. Similar impurity incorporation has been found for epitaxial laterally overgrown GaN on SiO<sub>2</sub>-mask by HVPE.<sup>24)</sup>

#### 4. Summary

We have shown a nano-scale direct one by one correlation of the structural and optical properties of GaN core-shell microrods fabricated by a combined bottom-up and top-down process. Threading dislocations generated during the MOVPE growth of GaN template on Si(111) propagate through the HVPE shell leading to a reduction of the panchromatic CL intensity due to non-radiative recombination processes. Probing the different growth regions of the shell from the as-grown core-shell microrods and the cross-

section TEM specimen, a strong difference of the local optical properties is observed. The strong incorporation of impurities during the epitaxial overgrowth by HVPE results in high free-carrier concentration in the non-polar shell region, which is evidenced by intense (e,h) recombination. In contrast, the center of the HVPE shell exhibits the donor-bound exciton emission and DAP transition, indicating a lower impurity concentration. Thus, the CL imaging gives a direct visualization of the impurity incorporation during the HVPE overgrowth of the MOVPE template.

### Acknowledgments

This research was supported by the German Research Foundation DFG. In particular, we gratefully acknowledge the Research Instrumentation Program INST 272/148-1 as well as the Collaborative Research Center SFB 787 “Semiconductor Nanophotonics: Materials, Models, Devices” and the “Materials World Network” program for financial support.

- 1) S. Li and A. Waag, *J. Appl. Phys.* **111**, 071101 (2012).
- 2) M. Mandl, X. Wang, T. Schimpke, C. Kölper, M. Binder, J. Ledig, A. Waag, X. Kong, A. Trampert, F. Bertram, J. Christen, F. Barbagini, E. Calleja, and M. Strassburg, *Phys. Status Solidi: Rapid Res. Lett.* **7**, 800 (2013).
- 3) A. Waag, X. Wang, S. Fündling, J. Ledig, M. Erenburg, R. Neumann, M. A. Suleiman, S. Merzsch, J. Wei, S. Li, H. H. Wehmann, W. Bergbauer, M. Straßburg, A. Trampert, U. Jahn, and H. Riechert, *Phys. Status Solidi C* **8**, 2296 (2011).
- 4) C. Kölper, M. Sabathil, F. Römer, M. Mandl, M. Strassburg, and B. Witzigmann, *Phys. Status Solidi A* **209**, 2304 (2012).
- 5) P. Waltereit, O. Brandt, A. Trampert, H. T. Grahn, J. Menni-ger, M. Ramsteiner, M. Reiche, and K. H. Ploog, *Nature* **406**, 865 (2000).
- 6) S. Albert, A. Bengoechea-Encabo, M. Sabido-Siller, M. Müller, G. Schmidt, S. Metzner, P. Veit, F. Bertram, M. A. Sánchez-García, J. Christen, and E. Calleja, *J. Cryst. Growth* **392**, 5 (2014).
- 7) H. Sekiguchi, K. Kishino, and A. Kikuchi, *Appl. Phys. Lett.* **96**, 231104 (2010).
- 8) M. Tchernycheva, P. Lavenus, H. Zhang, A. V. Babichev, G. Jacopin, M. Shahmohammadi, F. H. Julien, R. Ciecchonski, G. Vescovi, and O. Kryliouk, *Nano Lett.* **14**, 2456 (2014).
- 9) J. Hartmann, X. Wang, H. Schuhmann, W. Dziony, L. Caccamo, J. Ledig, M. Sadat Mohajerani, T. Schimpke, M. Baehr, G. Lilienkamp, W. Daum, M. Seibt, M. Straßburg, H. Wehmann, and A. Waag, *Phys. Status Solidi A* **212**, 2830 (2015).
- 10) H.-M. Kim, Y.-H. Cho, H. Lee, S. I. Kim, S. R. Ryu, D. Y. Kim, T. W. Kang, and K. S. Chung, *Nano Lett.* **4**, 1059 (2004).
- 11) S. Krylyuk, D. Paramanik, M. King, A. Motayed, J.-Y. Ha, J. E. Bonevich, A. Talin, and A. V. Davydov, *Appl. Phys. Lett.* **101**, 241119 (2012).
- 12) D. Paramanik, A. Motayed, G. S. Aluri, J.-Y. Ha, S. Krylyuk, A. V. Davydov, M. King, S. McLaughlin, S. Gupta, and H. Cramer, *J. Vac. Sci. Technol. B* **30**, 052202 (2012).
- 13) S. Krylyuk, R. Debnath, H. P. Yoon, M. R. King, J.-Y. Ha, B. Wen, A. Motayed, and A. V. Davydov, *APL Mater.* **2**, 106104 (2014).
- 14) Certain commercial equipment instruments or materials are identified in this paper to foster understanding. Such identification does not imply recommendation or endorsement by the National Institute of Standards and Technology nor does it imply that the materials or equipment identified are necessarily the best available for the purpose.
- 15) J. Christen, M. Grundmann, and D. Bimberg, *J. Vac. Sci. Technol. B* **9**, 2358 (1991).
- 16) F. Bertram, T. Riemann, J. Christen, A. Kaschner, A. Hoffmann, C. Thomsen, K. Hiramatsu, T. Shibata, and N. Sawaki, *Appl. Phys. Lett.* **74**, 359 (1999).
- 17) A. Urban, M. Müller, C. Karbaum, G. Schmidt, P. Veit, J. Malindretos, F. Bertram, J. Christen, and A. Rizzi, *Nano Lett.* **15**, 5105 (2015).
- 18) G. Schmidt, M. Müller, P. Veit, F. Bertram, J. Christen, M. Glauser, J.-F. Carlin, G. Cosendey, R. Butté, and N. Grandjean, *Appl. Phys. Lett.* **105**, 032101 (2014).
- 19) A. Dadgar, J. Bläsing, A. Diez, A. Alam, M. Heuken, and A. Krost, *Jpn. J. Appl. Phys.* **39**, L1183 (2000).
- 20) A. Kaschner, A. Hoffmann, C. Thomsen, F. Bertram, T. Riemann, J. Christen, K. Hiramatsu, H. Sone, and N. Sawaki, *Appl. Phys. Lett.* **76**, 3418 (2000).
- 21) B. Arnaudov, T. Paskova, E. M. Goldys, R. Yakimova, S. Evtimova, I. G. Ivanov, A. Henry, and B. Monemar, *J. Appl. Phys.* **85**, 7888 (1999).
- 22) B. Arnaudov, T. Paskova, E. M. Goldys, S. Evtimova, and B. Monemar, *Phys. Rev. B* **64**, 045213 (2001).
- 23) M. Feneberg, S. Osterburg, K. Lange, C. Lidig, B. Garke, R. Goldhahn, E. Richter, C. Netzel, M. D. Neumann, N. Esser, S. Fritze, H. Witte, J. Bläsing, A. Dadgar, and A. Krost, *Phys. Rev. B* **90**, 075203 (2014).
- 24) A. Kaschner, A. Hoffmann, C. Thomsen, F. Bertram, T. Riemann, J. Christen, K. Hiramatsu, T. Shibata, and N. Sawaki, *Appl. Phys. Lett.* **74**, 3320 (1999).
- 25) S. D. Hersee, A. K. Rishinaramangalam, and M. N. Fairchild, *J. Mater. Res.* **26**, 2293 (2011).
- 26) Y. Honda, Y. Iyechika, T. Maeda, H. Miyake, and K. Hiramatsu, *Jpn. J. Appl. Phys.* **40**, L309 (2001).
- 27) T. Riemann, T. Hempel, J. Christen, P. Veit, R. Clos, A. Dadgar, A. Krost, U. Habocek, and A. Hoffmann, *J. Appl. Phys.* **99**, 123518 (2006).
- 28) F. A. Ponce, D. P. Bour, W. Götz, and P. J. Wright, *Appl. Phys. Lett.* **68**, 57 (1996).
- 29) D. M. Hofmann, D. Kovalev, G. Steude, B. K. Meyer, A. Hoffmann, L. Eckey, R. Heitz, T. Detchprom, H. Amano, and I. Akasaki, *Phys. Rev. B* **52**, 16702 (1995).